Plasmon wave function of graphene nanoribbons

2015 New J. Phys. 17 083013

(http://iopscience.iop.org/1367-2630/17/8/083013)

New Journal of Physics
The open access journal at the forefront of physics

Deutsche Physikalische Gesellschaft DPG
IOP Institute of Physics

Published in partnership with: Deutsche Physikalische Gesellschaft and the Institute of Physics

OPEN ACCESS

RECEIVED
1 April 2015

REVISED
23 June 2015

ACCEPTED FOR PUBLICATION
29 June 2015

PUBLISHED
6 August 2015

PAPER

Plasmon wave function of graphene nanoribbons

I Silveiro[1], **J M Plaza Ortega**[1] **and F J García de Abajo**[1,2]

[1] ICFO-Institut de Ciencies Fotoniques, Mediterranean Technology Park, E-08860 Castelldefels (Barcelona), Spain
[2] ICREA-Institució Catalana de Recerca i Estudis Avançats, Passeig Lluís Companys 23, E-08010 Barcelona, Spain

E-mail: javier.garciadeabajo@icfo.es

Keywords: plasmon, graphene, nanophotonics

Abstract

We find the low-frequency optical response of highly doped individual and arrayed graphene nanoribbons to be accurately described in terms of plasmon wave functions (PWFs). More precisely, we focus on the lowest-order transverse dipolar mode, for which we define the wave function as the induced charge density associated with the plasmon. We show that a single universal wave function is capable of describing the normal-incidence interaction of paired, co-planar, and stacked arrays of ribbons down to small inter-ribbon distances. Our work provides both intuitive insight into graphene plasmon interactions and a practical way of accurately describing complex graphene geometries based on the PWFs of the individual components.

Doped graphene has emerged as an attractive alternative to noble metals for the study and manipulation of plasmons—collective oscillations of the conduction electrons—at infrared and THz frequencies [1–12]. Graphene plasmons possess unique advantages, such as long lifetimes [13, 14], strong nonlinearities [15–20], the ability of producing large optical field confinement and enhancement [20, 21], and an extraordinary electro-optical response, which allows us to spectrally [3, 4, 8, 10, 22] and spatially [5, 6] manipulate them via electrical gating. Because of these features, graphene plasmons have generated great expectations for their application in fields as diverse as light modulation [8, 10], nonlinear optics [15–18, 20], sensing [23, 24], and signal processing [2].

The large electro-optical response of graphene is related to its two-dimensional nature and electronic linear dispersion relation [25, 26], characterized by a uniform Fermi velocity $v_F \approx 10^6$ m s^{-1} and zero effective mass of its valence electrons. The Fermi energy $E_F = \hbar v_F \sqrt{\pi n}$ can be varied relative to the neutrality point by as much as 1 eV through the addition of moderate charge-carrier densities n of the order of one extra electron or hole per every 50 carbon atoms, which can be attained using chemical doping [27] or electrostatic gating [28, 29]. This is accompanied by the opening of a $2E_F$ optical gap, where collective plasmon modes can exist. Spectral and spatial control over these plasmons via electrical gating has been intensively investigated through experiment [3–8, 10, 30, 31] and theory [1, 13, 20, 21, 32–40], particularly in extended graphene [1, 13, 32], ribbons [21, 33–37], and finite nanoislands [20, 21, 38–40].

In this work, we introduce a simple analytical procedure to describe plasmon modes in graphene nanoribbons using the concept of the plasmon wave function (PWF), which we identify with the induced charge density associated with these modes. We obtain the PWF from classical electromagnetism for an individual ribbon, focusing for simplicity on the lowest-order transverse dipolar mode excited by a plane wave under normal incidence. The interaction between neighboring ribbons is then simulated with this wave function alone, conveniently normalized to represent a single plasmon. This simple PWF model allows us to accurately study the interaction between closely spaced ribbons forming dimers and periodic arrays in co-planar and stacked graphene configurations. The validity of our approach is tested by comparison with full numerical solutions of Maxwell's equations for dimers. Additionally, the PWF formalism allows us to deal with much shorter separations than a simpler dipole–dipole interaction model [38], while this limit is trivially reached at large distances. Our method is directly applicable to complex arrangements of arbitrary nanoisland morphologies, by simply using the wave functions of the plasmons encountered within the spectral range of interest.

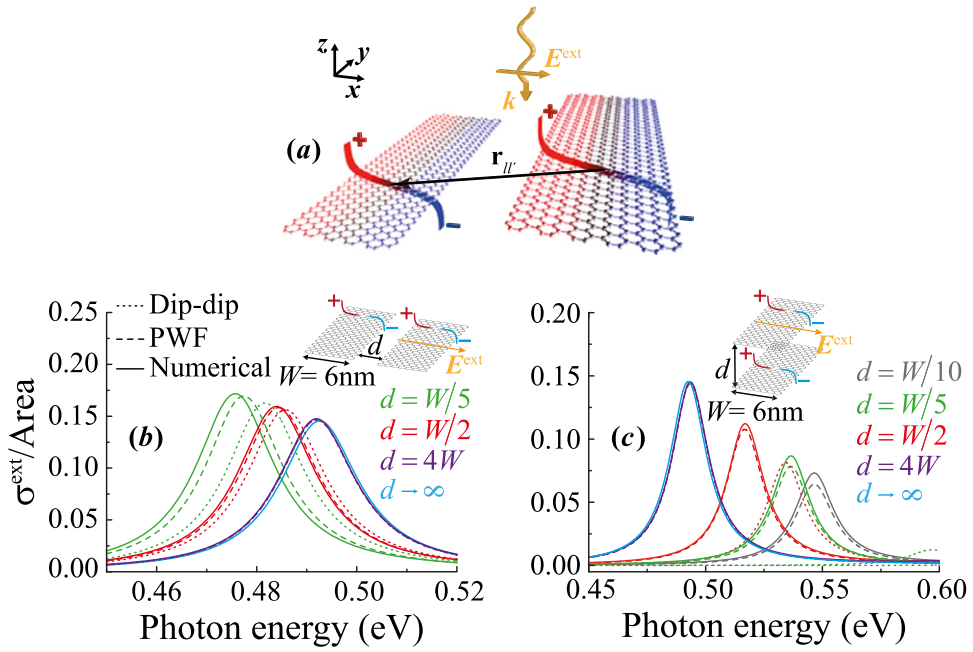

Figure 1. Plasmon wave functions (PWFs) and their interaction in graphene ribbon pairs. (a) We define the PWF as the induced charge density associated with the plasmon, which is illustrated in this sketch for two ribbons separated by a coordinate vector $\mathbf{r}_{ll'}$ and excited by a normal-incidence plane wave of transverse polarization. We concentrate on a spectral region dominated by the lowest-order transverse dipolar plasmon. (b), (c) Extinction cross-section normalized to the total graphene area of dimers formed by self-standing graphene nanoribbons separated by an edge-to-edge distance d in co-planar (b) and vertically-aligned (c) configurations. The ribbon width, Fermi energy, and damping are $W = 6$ nm, $E_F = 0.4$ eV, and $\hbar\gamma = 0.02$ eV, respectively. We compare full numerical solutions of the Maxwell equations (solid curves) with both the PWF (dashed curves) and the analytical dipole–dipole (dotted curves) models.

1. PWF model

The plasmon wavelength in graphene is typically much smaller than the light wavelength [22], so it is safe to describe the response of a given structure in the electrostatic limit. An eigenmode decomposition of this response [41] shows that it can be expressed in terms of the contribution arising from different plasmon resonances j. We consider a spectral region dominated by a single plasmon, corresponding to the lowest-order transverse mode of a ribbon $j = 1$, excited under normal incidence (see figure 1(a)). Now, we define the charge density ρ_1 associated with this plasmon as the PWF. The results presented below are then based on the use of a single universal function ρ_1, which we obtain by numerically solving the electromagnetic problem using previously discussed methods [42].

When we consider several ribbons aligned along y (figure 1(a)), the excitation of the plasmon in a given ribbon l produces an induced line dipole p_l along x. The self-consistent interaction between the plasmons of different ribbons is then described by

$$p_l = \alpha_\omega \left(E^{\text{ext}} + \sum_{l' \neq l} \mathcal{G}_{ll'} p_{l'} \right), \tag{1}$$

where α_ω is the single-ribbon polarizability (see appendix B, equation (B.5)) and $\mathcal{G}_{ll'}$ describes the coupling between ribbons l and l' separated by a coordinate vector $\mathbf{r}_{ll'}$. The latter is essentially given by the Coulomb interaction between their respective PWFs,

$$\mathcal{G}_{ll'} = \frac{-1}{\zeta_1^2} \int \mathrm{d}^2\mathbf{R} \int \mathrm{d}^2\mathbf{R}' \frac{\rho_1(\mathbf{R})\rho_1(\mathbf{R}')}{|\mathbf{R} - \mathbf{R}' - \mathbf{r}_{ll'}|}, \tag{2}$$

which is normalized using the dipolar mode strength $\zeta_1 = \int x\rho_1(\mathbf{R})\,\mathrm{d}^2\mathbf{R}$. This constitutes a generalization with respect to a dipole–dipole model based upon the long-distance limit of equation (2) (i.e., large $r_{ll'}$ compared with the ribbon width), which produces the well-known expression $\mathcal{G}_{ll'} \approx 3x_l x_{l'}/r_{ll'}^5 - 1/r_{ll'}^3$ and has been discussed elsewhere in the context of graphene [37]. Further details of the PWF formalism are given in the appendix A, where we present a self-consistent derivation for arbitrary arrangements of aligned ribbons. Next, we study ribbon pairs and periodic arrays in different configurations by comparing full electromagnetic solutions [42] with both the PWF and the dipole–dipole models. The graphene response is described in the local-RPA

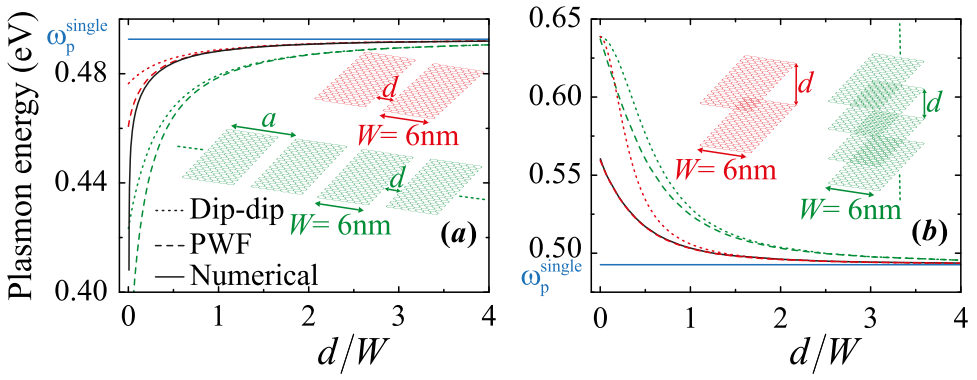

Figure 2. Plasmon energy of interacting graphene ribbons in different dimer and array configurations. (**a**) Evolution of the plasmon energies with edge-to-edge separation in co-planar ribbon dimers (red curves) and infinite ribbon arrays (green curves), aligned as shown in the insets. The black solid curve corresponds to the full numerical calculation for the dimers. The ribbon width is $W = 6$ nm and the Fermi energy is $E_F = 0.4$ eV. (b) Same as (a) for vertically offset ribbons (the legend is the same as in (a)).

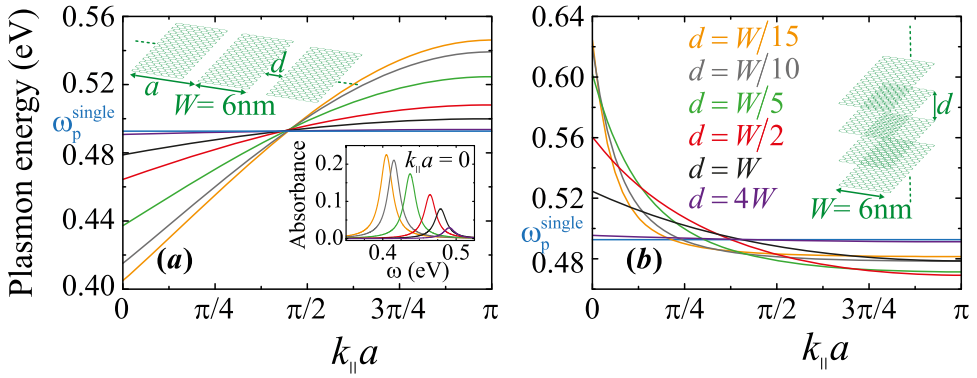

Figure 3. Dispersion relation of graphene ribbon arrays. (a) We show the dispersion relation obtained with the PWF model for co-planar arrays of period $a = W + d$ (see upper inset). The ribbon width is $W = 6$ nm, the Fermi energy is $E_F = 0.4$ eV, and the edge-to-edge separation d is varied as indicated in the legend of (b). The lower inset shows the normal-incidence absorbance ($k_\parallel = 0$) for a damping $\hbar\gamma = 0.02$ eV. (b) Same as (a) for arrays of vertically stacked ribbons of period $a = d$.

approximation [21] in all cases. For comparison, we also offer calculations similar to those of figures 2 and 3 using the Drude response model in figures B1 and C1 of the appendix.

2. Ribbon dimers

We start by analyzing the plasmons sustained by two neighboring ribbons of small width $W = 6$ nm and Fermi energy $E_F = 0.4$ eV, in either co-planar (figure 1(b)) or vertically stacked (figure 1(c)) configurations. We show the extinction cross-section obtained from the optical theorem. These systems display a prominent plasmon that starts at the single-ribbon energy at large separations and undergoes dramatic redshifts (blueshifts) due to inter-ribbon attractive (repulsive) interaction in co-planar (stacked) arrangements, as shown in figure 1(b) (figure 1(c)). The positive (negative) character of this interaction is intuitively suggested from the induced charge distribution shown in figure 1(a). Remarkably, the PWF model (dashed curves) agrees well with the full numerical solution (solid curves) down to very small separations. In contrast, the dipole–dipole model only produces accurate results at large separations, and its failure at small distances is particularly severe for stacked ribbons. This behavior is clearly observed in the distance dependence of the dimer plasmon energy, which is summarized in figure 2, as obtained from the zeros of $\mathrm{Re}\{\alpha_\omega^{-1} - \mathcal{G}\}$. Incidentally, using the Drude model for the conductivity (see figure B1 in the appendix B) the stacked dimer plasmon smoothly converges to roughly the frequency of a single ribbon with double the conductivity within the PWF model, which leads to $\omega_p/\omega_p^{single} \approx \sqrt{2}$ at $d = 0$; this result, which essentially stems from the fact that the plasmon energy is proportional to $\sqrt{E_F}$ in the Drude model, is however not attained in the dipole–dipole model.

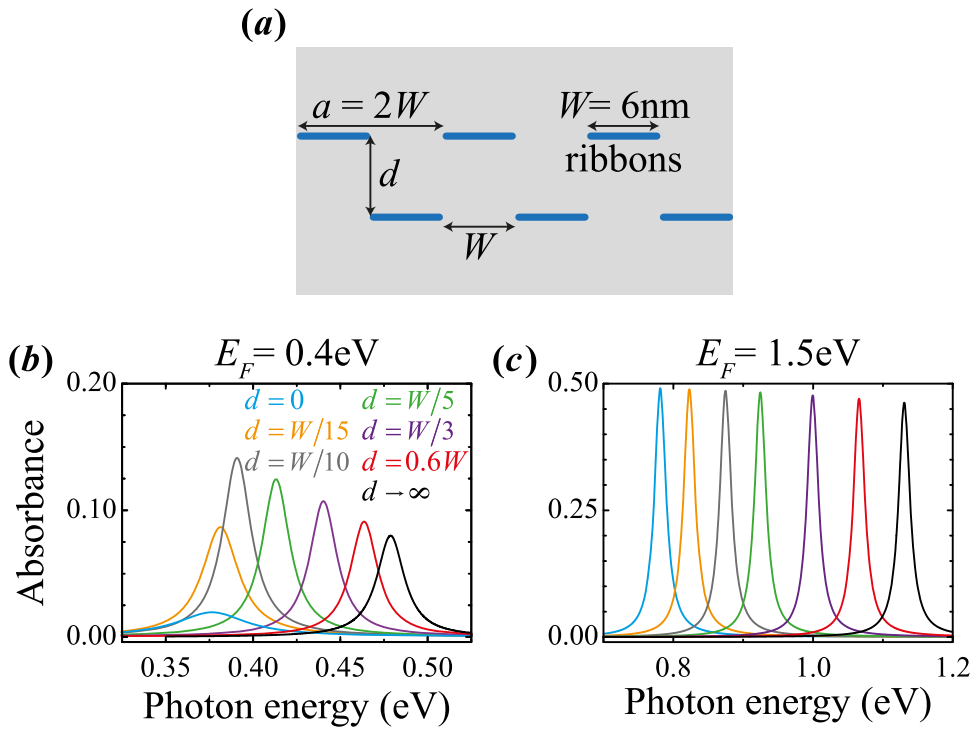

Figure 4. Bilayer ribbon array. (a) Cross section of the structure under consideration. (b), (c) Normal-incidence absorbance for several interlayer distances and two different Fermi energies. The damping is $\hbar\gamma = 0.02$ eV.

3. Periodic ribbon arrays

A similar analysis for periodic arrays in both co-planar (figure 3(a)) and vertically stacked (figure 3(b)) configurations reveals larger frequency shifts due to inter-ribbon interaction than in dimers. Under normal incidence, the dipoles of different ribbons are identical, so equation (1) can be analytically solved by summing $G = \sum_{l\neq 0} \mathcal{G}_{0\,l}$, leading again to semi-analytical results for the plasmon frequency (obtained from $\mathrm{Re}\{\alpha_\omega^{-1} - G\} = 0$) and the absorbance (see appendix C). The PWF model also allows us to obtain the plasmonic bands of these periodic structures as a function of wave vector $k_\parallel$ along the array direction, so that $p_l \propto \mathrm{e}^{\mathrm{i}k_\parallel a l}$, where a is the period, and we have to rewrite $G = \sum_{l\neq 0} \mathcal{G}_{0\,l}\mathrm{e}^{\mathrm{i}k_\parallel a l}$ (see figure 3). As expected, the bands are very flat at large separations, where the plasmons are well localized at the ribbons, but they acquire significant dispersion at short distances, indicating the presence of more delocalized plasmons that can propagate along the array.

As a final illustration of the power of the PWF model, we explore in figure 4 the absorbance of two neighboring layers of graphene ribbon arrays with a lateral offset. The spectra are dominated by a single plasmon feature, which redshifts with decreasing interlayer distance due to attractive interaction similar to the dimers, as discussed above. Interestingly, there is a clear dependence of the near-touching behavior on the Fermi energy (see figures 4(b) and (c)), although nonlocal effects can be important in this limit [43], which could be dealt with by reformulating the present classical formalism in terms of an atomistic description of the PWFs.

4. Outlook and conclusion

We have shown that the concept of PWF (i.e., the induced charge density associated with the plasmon) captures the details of the interaction between plasmonic structures in close proximity. For simplicity, we have limited our analysis to arrangements of graphene ribbons, but this model can be easily adapted to deal with other geometries and incorporate more plasmon modes in each structure. The PWF model constitutes a natural extension of the popular dipole–dipole interaction model, combining its ability to produce analytical expressions with a better degree of accuracy. While it can in principle deal with arbitrary distributions of plasmonic systems, it is particularly suited to understand and design nanostructures based on 2D plasmonic materials such as graphene.

Acknowledgments

This work is partially supported by the European Commission (Graphene Flagship CNECT-ICT-604391 and FP7-ICT-2013-613024-GRASP).

Appendix A. Electrostatic eigenmode expansion and PWF

We study the optical response of graphene ribbons aligned with their long axis along the y direction and oriented perpendicularly with respect to z. The ribbons are illuminated by a normal-incidence monochromatic plane wave of external field $\mathbf{E}^{\rm ext}(\mathbf{r},\, t) = E^{\rm ext}e^{-i\omega(z/c+t)}\hat{\mathbf{x}}$ + c.c. (transversal polarization). We focus on the $e^{-i\omega t}$ component in what follows, keeping in mind that the full time dependence of all magnitudes under consideration is obtained as the real part multiplied by 2. The width of the ribbons is small compared with the light wavelength, and therefore, we analyze their response in the electrostatic limit, inspired in an eigenmode expansion formalism discussed elsewhere [37]. The system possesses translational symmetry, so the y component of the electric field is zero. We can formulate a self-consistent equation for the remaining in-plane component,

$$E_x(x,\,\omega) = E^{\rm ext} + \frac{i}{\omega}\frac{\partial}{\partial x}\int\!\!\int \frac{dx'dy}{\sqrt{(x-x')^2+y^2}}\left[\frac{\partial}{\partial x'}\sigma(x',\,\omega)E_x(x',\,\omega)\right], \tag{A.1}$$

where the integral represents the induced scalar potential and the expression in the square brackets is the induced density, which is in turn written in terms of the current via the continuity equation, using the two-dimensional, local, space- and frequency-dependent graphene conductivity $\sigma(x,\,\omega)$. We further assume the factorization $\sigma(x,\,\omega) = f(\theta)\sigma(\omega)$, where $f(\theta)$ is 1 on the graphene and 0 elsewhere. Here, we have used a dimensionless coordinate $\theta = x/W$, where W is the ribbon width. We now define

$$\mathcal{E}(\theta,\,\omega) = W\sqrt{f(\theta)}\;E_x(\theta,\,\omega),$$

which is subject, from equation (A.1), to the self-consistent relation

$$\mathcal{E}(\theta,\,\omega) = \mathcal{E}^{\rm ext} + \eta(\omega)\int d\theta'\; M(\theta,\,\theta')\mathcal{E}(\theta',\,\omega), \tag{A.2}$$

where $\eta(\omega) = i\sigma(\omega)/\omega W$ and $M(\theta,\,\theta') = -2\sqrt{f(\theta)f(\theta')}\;\partial^2(\log|\theta-\theta'|)\big/\partial\theta^2$. The linear operator M is clearly real and symmetric, so it admits real eigenvalues $1/\eta_j$ and eigenvectors $\mathcal{E}_j$ that satisfy

$$\mathcal{E}_j(\theta) = \eta_j\int d\theta'\; M(\theta,\,\theta')\mathcal{E}_j(\theta') \tag{A.3}$$

and form a complete and orthonormal basis set

$$\int d\theta\;\mathcal{E}_j(\theta)\mathcal{E}_{j'}(\theta) = \delta_{jj'}. \tag{A.4}$$

This allows us to readily solve equation (A.2) as

$$\mathcal{E}(\theta,\,\omega) = \sum_j \frac{c_j}{1-\eta(\omega)/\eta_j}\,\mathcal{E}_j(\theta), \tag{A.5}$$

with expansion coefficients $c_j = WE^{\rm ext}\int d\theta\sqrt{f(\theta)}\;\mathcal{E}_j(\theta)$.

At this point, it is convenient to introduce the PWF associated with mode j,

$$\rho_j(\theta) = \frac{\partial}{\partial\theta}\sqrt{f(\theta)}\,\mathcal{E}_j(\theta),$$

in terms of which the expansion coefficients of equation (A.5) reduce to

$$c_j = -WE^{\rm ext}\zeta_j,$$

where

$$\zeta_j = \int d\theta\;\theta\;\rho_j(\theta). \tag{A.6}$$

It should be noted that ρ_j is proportional to the induced charge of mode j, whereas ζ_j can be regarded as the normalized dipole moment.

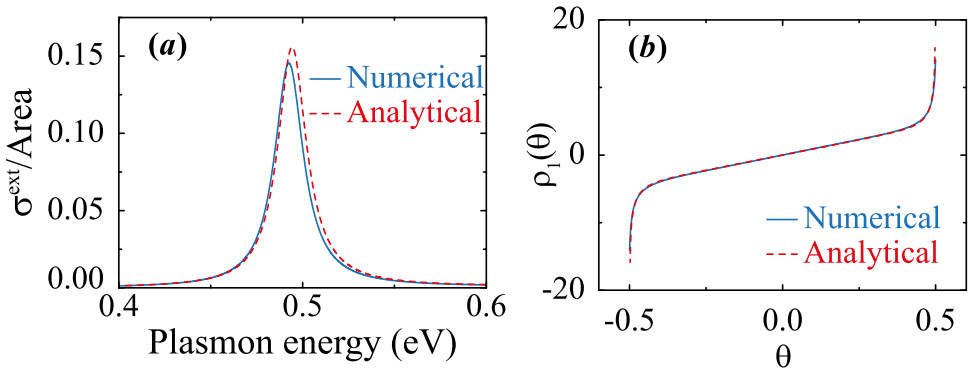

Figure A1. Plasmon resonance (a) and PWF (b) for the lowest-order transversal mode of a graphene ribbon. The width and graphene parameters are the same as in the ribbons of figure 1. Full numerical simulations [42] (solid curves) are compare with analytical fits (dashed curves). In (a) the extinction cross-section is fitted to $\sigma^{\rm ext}(\omega) = (4\pi\omega/c)\,{\rm Im}\{\alpha_\omega\}$ (dashed curve) with α_ω given by equation (B.5). The fitting coefficients are $\eta_1 \approx -0.069$ and $\zeta_1 \approx 0.94$. In (b) the PWF is obtained from the calculated induced charge density at the frequency of the extinction maximum, and it is well approximated by the phenomenological analytical function $\rho_1(\theta) \approx 9\,\theta\left[1 + 0.25\,{\rm e}^{-5+20\theta^2}(1-4\theta^2)^{-1/2}\right]$ (dashed curve), where $\theta = x/W$ and W is the ribbon width. The numerical prefactor is adjusted so that the above value of ζ_1 is generated by equation (A.6) when using this function $\rho_1(\theta)$.

Appendix B. Interaction between ribbons

For simplicity, we study the response of identical ribbons within a spectral region dominated by their lowest-order transversal dipole plasmon ($j = 1$), so we neglect other modes in what follows. We show the density profile of this plasmon in figure A1, as obtained by numerically solving the electromagnetic problem [42]. We can decompose $\mathcal{E}$ as a sum of contributions from different ribbons

$$\mathcal{E}(\theta,\,\omega) = \sum_l d_l\;\mathcal{E}_1\big(\theta - \theta_l\big), \tag{B.1}$$

where θ_l indicates the position of a central point in ribbon l. Inserting equation (B.1) into equation (A.2), and using equations (A.3) and (A.4), we find the self-consistent equation

$$d_l = \frac{1}{1-\eta(\omega)/\eta_1}\left[-WE^{\rm ext}\zeta_1 + \eta(\omega)\sum_{l'\neq l} M_{ll'}d_{l'}\right] \tag{B.2}$$

for the expansion coefficients, where

$$\begin{aligned} M_{ll'} &= \int {\rm d}\theta \int {\rm d}\theta'\;\mathcal{E}_1\big(\theta-\theta_l\big)M(\theta,\theta')\mathcal{E}_{l'}\big(\theta'-\theta_{l'}\big) \\ &= \int {\rm d}\theta \int {\rm d}\theta'\;\rho_1(\theta)\rho_1(\theta')\;\log\left[\big(\theta-\theta'+\theta_l-\theta_{l'}\big)^2 + (z_l-z_{l'})^2\big/W^2\right] \end{aligned} \tag{B.3}$$

describes the interaction between ribbons l and l'. Notice that we have generalized $M_{ll'}$ in order to deal with ribbons that are located at different heights z_l.

Using the expression in the square brackets of equation (A.1) to calculate the induced charge (i.e., $\rho^{\rm ind} = (-\eta/W)\partial(\sqrt{f}\mathcal{E})\big/\partial\theta$), we readily find the dipole moment induced on ribbon l per unit length along the direction of translational symmetry

$$p_l = -\eta W d_l \zeta_1.$$

It is then convenient to rewrite equation (B.2) in terms of these dipoles as

$$p_l = \alpha_\omega\left(E^{\rm ext} + \sum_{l'\neq l}\mathcal{G}_{ll'}p_{l'}\right), \tag{B.4}$$

where

$$\mathcal{G}_{ll'} = \frac{M_{ll'}}{W^2\zeta_1^2}$$

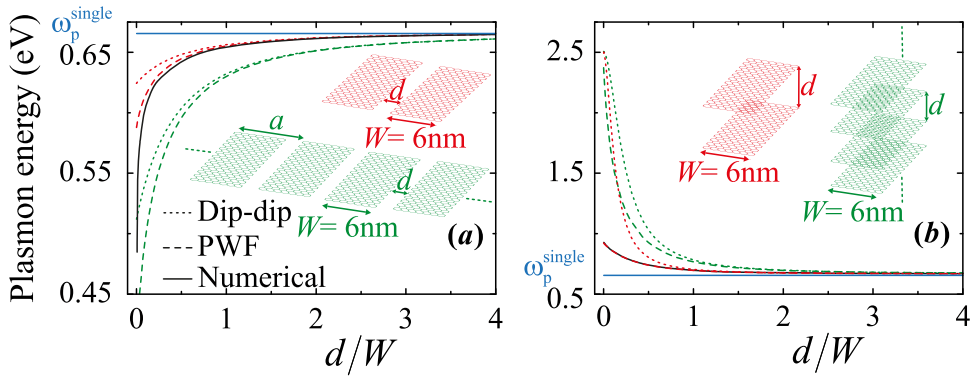

Figure B1. Same as figure 2, but using the Drude conductivity $\sigma(\omega) = (ie^2E_F/\pi\hbar^2)/(\omega + i\gamma)$.

describes the dipole–dipole interaction, whereas

$$\alpha_\omega = \frac{W^2\zeta_1^2}{1/\eta(\omega) - 1/\eta_1} \tag{B.5}$$

is the ribbon polarizability per unit length in the single-mode approximation.

We are interested in the extinction cross-section, which can be calculated from the induced dipoles using the optical theorem [44] as

$$\sigma^{ext}(\omega) = \frac{4\pi\omega}{c}\ \mathrm{Im}\left\{\sum_l p_l \Big/ E^{ext}\right\}. \tag{B.6}$$

Inverting equation (B.4), we can rewrite equation (B.6) as

$$\sigma^{ext}(\omega) = \frac{4\pi\omega}{c}\sum_{ll'}\mathrm{Im}\left\{\frac{1}{\alpha_\omega^{-1} - \mathcal{G}}\Bigg|_{ll'}\right\},$$

where $\mathcal{G}$ is a matrix of elements $(1 - \delta_{ll'})\mathcal{G}_{ll'}$.

The plasmon frequency of two interacting ribbons ($l = 1, 2$) is represented in figure 2 using the local-RPA surface conductivity and in figure B1 using the Drude model, as calculated from the condition $\mathrm{Re}\{\alpha_\omega^{-1} - \mathcal{G}_{12}\} = 0$.

Appendix C. Periodic arrays

In periodic arrays, $p_l \equiv p$ is independent of l, so we can solve equation (B.4) as

$$p = \frac{E^{ext}}{\alpha_\omega^{-1} - G},$$

where $G = \sum_{l\neq 0}\mathcal{G}_{0l}$. In particular, for an array of co-planar ribbons, the reflection coefficient derived from this expression reduces to [37]

$$r = \frac{iS}{\alpha_\omega^{-1} - G - iS},$$

where $S = 2\pi\omega/ac$ accounts for the coupling to propagating light and a is the lattice period. Incidentally, we have introduced the $-iS$ term in the denominator in order to describe radiative damping in the dipole–dipole limit [37]. Finally, the absorbance of the array reduces to $1 - |r|^2 - |t|^2$, where $t = 1 + r$ is the transmission coefficient.

The plasmon frequency of ribbon arrays is also represented in figures 2 and B1 as calculated from the condition $\mathrm{Re}\{\alpha_\omega^{-1} - G\} = 0$. Furthermore, we show dispersion relations for ribbon arrays in figures 3 and C1, which are obtained by including the dependence on the wave vector component along the direction of periodicity $k_\parallel$ through $G = \sum_{l\neq 0}\mathcal{G}_{0l}e^{ik_\parallel al}$.

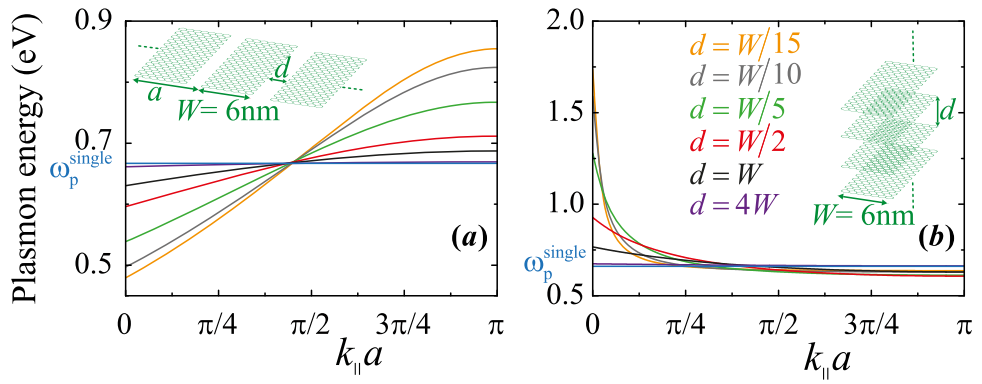

Figure C1. Same as figure 3, but calculated for the Drude conductivity $\sigma(\omega) = (ie^2E_F/\pi\hbar^2)/(\omega + i\gamma)$.

Appendix D. Dipole–dipole model

In the long distance limit, $\Delta_{ll'} \equiv \left[(x_l - x_{l'})^2 + (z_l - z_{l'})^2\right]/W^2 \gg 1$, we can expand the Coulomb interaction described by the log function of equation (B.3) in powers of $1/\Delta_{ll'}$. The monopolar and dipolar terms vanish in virtue of the neutrality of the PWF (i.e., $\int d\theta\, \rho_1(\theta) = 0$), so the leading contribution reduces to the well-known dipole–dipole term, which reads

$$\mathcal{G}_{ll'} \approx 2\frac{(z_l - z_{l'})^2 - (x_l - x_{l'})^2}{\left[(z_l - z_{l'})^2 + (x_l - x_{l'})^2\right]^2}.$$

For co-planar and vertically stacked dimers separated by a center-to-center distance d, we have $\mathcal{G}_{12} = -2/d^2$ and $2/d^2$, respectively. For periodic arrays of co-planar ribbons and period a, we have $x_l = la$ and $z_l = 0$, leading to $\mathcal{G}_{0\,l} = -2/(la)^2$, so we obtain $G = -2\pi^2/3a^2$. Likewise, for vertically stacked ribbons of period a (i.e., $x_l = 0$ and $z_l = la$), we find G to be exactly the opposite of this value.

References

[1] Hwang E H and das Sarma S 2007 Dielectric function, screening, and plasmons in two-dimensional graphene *Phys. Rev.* B **75** 205418
[2] Vakil A and Engheta N 2011 Transformation optics using graphene *Science* **332** 1291–4
[3] Ju L *et al* 2011 Graphene plasmonics for tunable terahertz metamaterials *Nat. Nanotechnol.* **6** 630–4
[4] Fei Z *et al* 2011 Infrared nanoscopy of dirac plasmons at the graphene–sio$_2$ interface *Nano. Lett.* **11** 4701–5
[5] Chen J *et al* 2012 Optical nano-imaging of gate-tunable graphene plasmons *Nature* **487** 77–81
[6] Fei Z *et al* 2012 Gate-tuning of graphene plasmons revealed by infrared nano-imaging *Nature* **487** 82–85
[7] Yan H, Li X, Chandra B, Tulevski G, Wu Y, Freitag M, Zhu W, Avouris P and Xia F 2012 Tunable infrared plasmonic devices using graphene/insulator stacks *Nat. Nanotechnol.* **7** 330–4
[8] Brar V W, Jang M S, Sherrott M, Lopez J J and Atwater H A 2013 Highly confined tunable mid-infrared plasmonics in graphene nanoresonators *Nano Lett.* **13** 2541–7
[9] Yan H, Low T, Zhu W, Wu Y, Freitag M, Li X, Guinea F, Avouris P and Xia F 2013 Damping pathways of mid-infrared plasmons in graphene nanostructures *Nat. Photon.* **7** 394–9
[10] Fang Z, Thongrattanasiri S, Schlather A, Liu Z, Ma L, Wang Y, Ajayan P M, Nordlander P, Halas N J and García de Abajo F J 2013 Gated tunability and hybridization of localized plasmons in nanostructured graphene *ACS Nano* **7** 2388–95
[11] Rodin A S, Fei Z, McLeod A S, Wagner M, Castro Neto A H, Fogler M M and Basov D N 2013 Plasmonic hot spots in triangular tapered graphene microcrystals arXiv:1309.1909
[12] Jang M S, Brar V W, Sherrott M C, Lopez J J, Kim L, Kim S, Choi M and Atwater H A 2014 Tunable large resonant absorption in a midinfrared graphene salisbury screen *Phys. Rev.* B **90** 165409
[13] Jablan M, Buljan H and Soljačić M 2009 Plasmonics in graphene at infrared frequencies *Phys. Rev.* B **80** 245435
[14] Principi A, Carrega M, Lundeberg M B, Woessner A, Koppens F H L, Vignale G and Polini M 2014 Plasmon losses due to electron-phonon scattering: the case of graphene encapsulated in hexagonal boron nitride *Phys. Rev.* B **90** 165408
[15] Mikhailov S A 2007 Non-linear electromagnetic response of graphene *Europhys. Lett.* **79** 27002
[16] Mikhailov S A 2008 Electromagnetic response of electrons in graphene: nonlinear effects *Physica* E **40** 2626–9
[17] Hendry E, Hale P J, Moger J, Savchenko A K and Mikhailov S A 2010 Coherent nonlinear optical response of graphene *Phys. Rev. Lett.* **105** 097401
[18] Mikhailov S A 2011 Theory of the giant plasmon-enhanced second-harmonic generation in graphene and semiconductor two-dimensional electron systems *Phys. Rev.* B **84** 045432
[19] Cox J D and García de Abajo F J 2014 Electrically tunable nonlinear plasmonics in graphene nanoislands *Nat. Commun.* **5** 5725
[20] Novotny L and Hecht B 2006 *Principles of Nano-Optics* (New York: Cambridge University Press)
[21] Koppens F H L, Chang D E and García de Abajo F J 2011 Graphene plasmonics: a platform for strong light–matter interactions *Nano Lett.* **11** 3370–7

[22] Fang Z, Wang Y, Schlather A, Liu Z, Ajayan P M, García de Abajo F J, Nordlander P, Zhu X and Halas N J 2014 Active tunable absorption enhancement with graphene nanodisk arrays *Nano Lett.* **14** 299–304
[23] Shen J, Zhu Y, Yang X and Li C 2012 Graphene quantum dots: emergent nanolights for bioimaging, sensors, catalysis and photovoltaic devices *Chem. Commun.* **48** 3686–99
[24] Rodrigo D, Limaj O, Janner D, Etezadi D, García de Abajo F J, Pruneri V and Altug H 2015 Mid-infrared biosensing with graphene *Science* **349** 165–8
[25] Wallace P R 1947 The band theory of graphite *Phys. Rev.* **71** 622–34
[26] Castro Neto A H, Guinea F, Peres N M R, Novoselov K S and Geim A K 2009 The electronic properties of graphene *Rev. Mod. Phys.* **81** 109–62
[27] Khrapach I, Withers F, Bointon T H, Polyushkin D K, Barnes W L, Russo S, Craciun M F and Monica F 2012 Novel highly conductive and transparent graphene-based conductors *Adv. Mater.* **24** 2844–9
[28] Efetov D K and Kim P 2010 Controlling electron–phonon interactions in graphene at ultrahigh carrier densities *Phys. Rev. Lett.* **105** 256805
[29] Chen C F, Park C H, Boudouris B W, Horng J, Geng B, Girit C, Zettl A, Crommie M F, Segalman R A, Louie S G and Wang F 2011 Controlling inelastic light scattering quantum pathways in graphene *Nature* **471** 617–20
[30] Shin S Y, Kim N D, Kim J G, Kim K S, Noh D Y, Kim Kwang S and Chung J W 2011 Control of the π plasmon in a single layer graphene by charge doping *Appl. Phys. Lett.* **99** 082110
[31] Yan H, Li Z, Li X, Zhu W, Avouris P and Xia F 2012 Infrared spectroscopy of tunable dirac terahertz magneto-plasmons in graphene *Nano Lett.* **12** 3766–71
[32] Wunsch B, Stauber T, Sols F and Guinea F 2006 Dynamical polarization of graphene at finite doping *New J. Phys.* **8** 318
[33] Brey L and Fertig H A 2007 Elementary electronic excitations in graphene nanoribbons *Phys. Rev.* B **75** 125434
[34] Nikitin A Y, Guinea F, García-Vidal F J and Martín-Moreno L 2011 Edge and waveguide terahertz surface plasmon modes in graphene microribbons *Phys. Rev.* B **84** 161407
[35] Thongrattanasiri S, Silveiro I and García de Abajo F J 2012 Plasmons in electrostatically doped graphene *Appl. Phys. Lett.* **100** 201105
[36] Wang W and Kinaret J M 2013 Plasmons in graphene nanoribbons: interband transitions and nonlocal effects *Phys. Rev.* B **87** 195424
[37] García de Abajo F J 2014 Graphene plasmonics: Challenges and opportunities *ACS Photon.* **1** 135–52
[38] Thongrattanasiri S, Koppens F H L and García de Abajo F J 2012 Complete optical absorption in periodically patterned graphene *Phys. Rev. Lett.* **108** 047401
[39] Manjavacas A, Thongrattanasiri S and García de Abajo F J 2013 Plasmons driven by single electrons in graphene nanoislands *Nanophotonics* **2** 139–51
[40] Silveiro I and García de Abajo F J 2014 Plasmons in inhomogeneously doped neutral and charged graphene nanodisks *Appl. Phys. Lett.* **104** 131103
[41] García de Abajo F J 2013 Multiple excitation of confined graphene plasmons by single free electrons *ACS Nano* **7** 11409–19
[42] Christensen J, Manjavacas A, Thongrattanasiri S, Koppens F H L and García de Abajo F J 2012 Graphene plasmon waveguiding and hybridization in individual and paired nanoribbons *ACS Nano* **6** 431–40
[43] Silveiro I, Plaza Ortega J M and García de Abajo F J 2015 Quantum nonlocal effects in individual and interacting graphene nanoribbons *Light Sci. Appl.* **4** e241
[44] Jackson J D 1999 *Classical Electrodynamics* (New York: Wiley)